# Table of Contents

# Appendix Figure S1. Knockdown efficiencies and cellular viabilities upon CBX4 depletion.

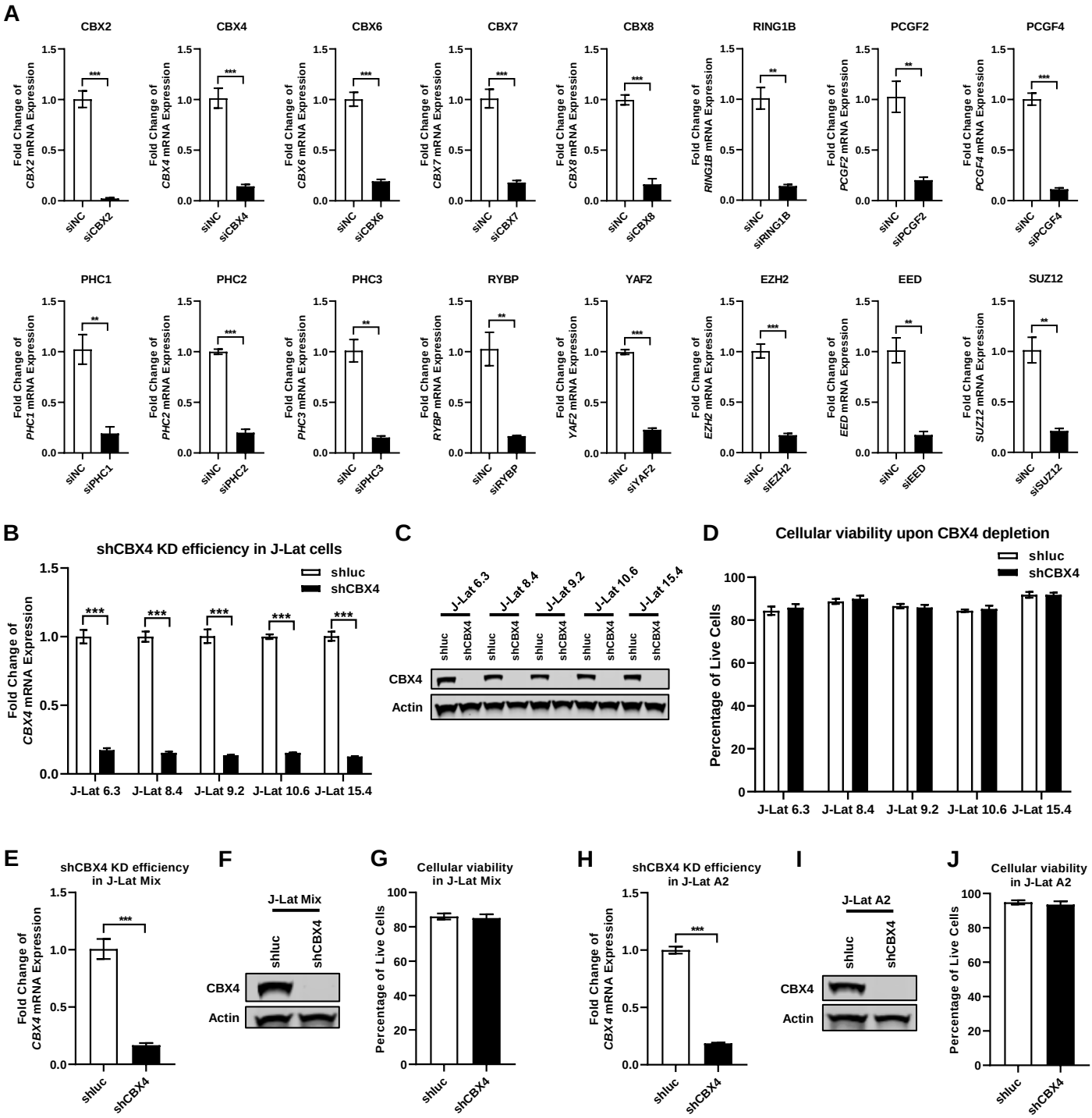

**Appendix Figure S1. Knockdown efficiencies and cellular viabilities upon CBX4 depletion.**

**A.** Knockdown efficiencies of different genes within the siRNA library. The relative expression of each gene in siTarget group was quantified by RT-qPCR and normalized to siNC group.

**B, C.** The shCBX4 knockdown efficiencies of CBX4 in J-Lat 6.3, 8.4, 9.2, 10.6 and 15.4 were evaluated by both RT-qPCR (B) and western blot (C).

**D.** Cellular viabilities upon CBX4 knockdown in latency cell lines including J-Lat 6.3, 8.4, 9.2, 10.6 and 15.4 were quantitated by measuring the percentages of amine-reactive fluorescent dye non-permeant cells.

**E, F.** The shCBX4 knockdown efficiencies of CBX4 in J-Lat Mix were evaluated by both RT-qPCR (E) and western blot (F).

**G.** Cellular viabilities upon CBX4 knockdown in J-Lat Mix were quantitated as in (D).

**H, I.** The shCBX4 knockdown efficiencies of CBX4 in J-Lat A2 were evaluated by both RT-qPCR (H) and western blot (I).

**J.** Cellular viabilities upon CBX4 knockdown in J-Lat A2 were quantitated as in (D).

Data information: Data represented mean ± SEM in biological triplicate. p-Values in (A), (B), (D), (E), (G), (H) and (J) were calculated by Student's *t*-test. **p < 0.01, ***p < 0.001.

**Appendix Figure S2. CBX4 knockdown efficiency and cellular viability in ChIP samples.**

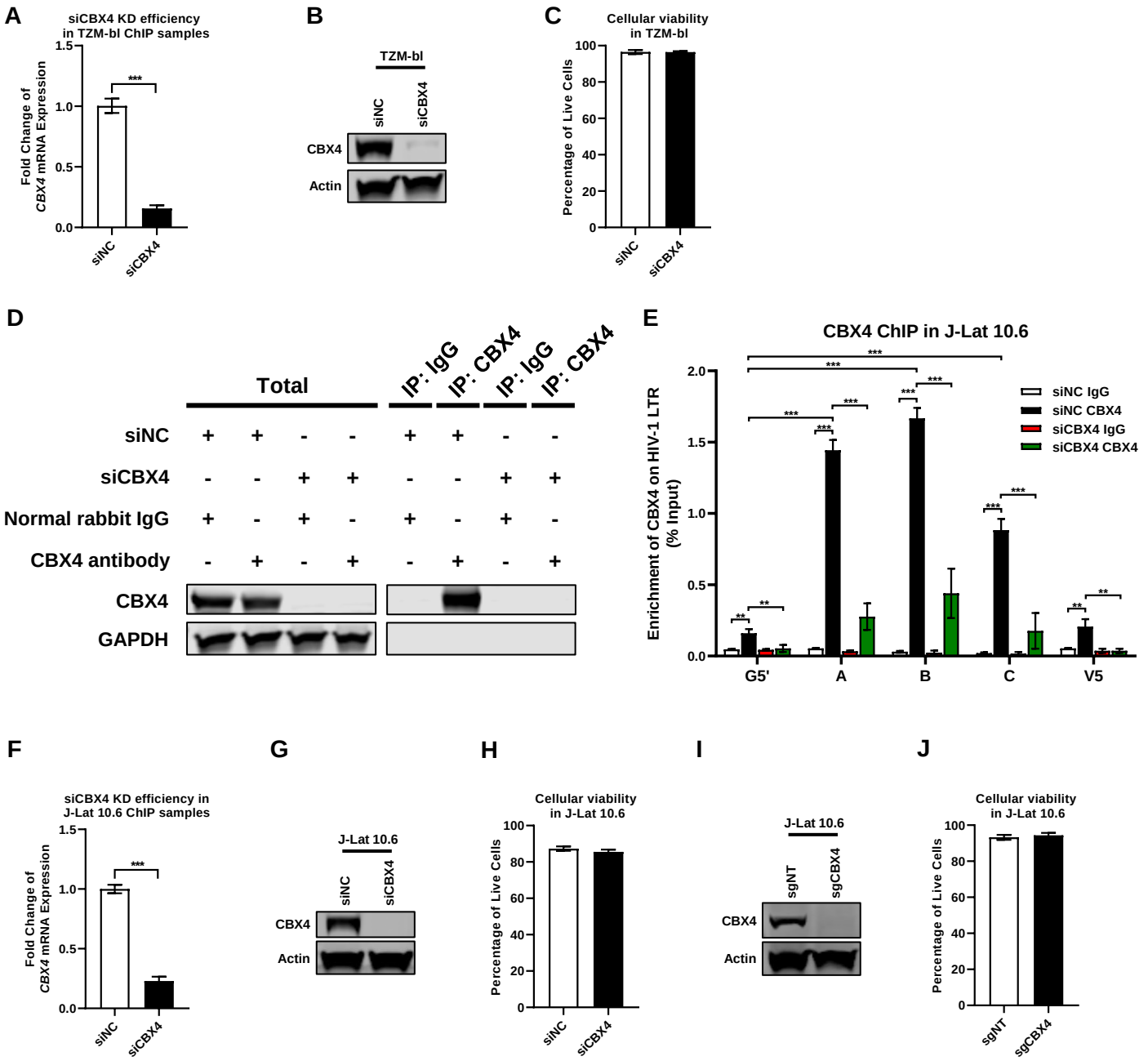

**Appendix Figure S2. CBX4 knockdown efficiency and cellular viability in ChIP samples.**

**A-C.** siCBX4-mediated CBX4 knockdown efficiencies in TZM-bl cells were evaluated by both RT-qPCR (A) and western blot (B). Cellular viabilities upon CBX4 knockdown in TZM-bl cells were quantitated by measuring the percentages of amine-reactive fluorescent dye non-permeant cells (C).

**D.** The IP efficiencies of CBX4 antibodies in both siNC- and siCBX4-treated TZM-bl cells were evaluated by western blot.

**E.** ChIP assays with antibodies against IgG and CBX4 were performed in both siNC-treated and siCBX4-treated J-Lat 10.6 cells. Five pairs of ChIP-qPCR primers were designed as in Fig 2A. G5' represented cellular DNA and viral 5'LTR junction in J-Lat 10.6. ChIP-qPCR DNA signals were normalized to Input.

**F-H.** siCBX4-mediated CBX4 knockdown efficiencies in J-Lat 10.6 cells were evaluated by both RT-qPCR (F) and western blot (G). Cellular viabilities upon CBX4 knockdown were evaluated by measuring the percentages of amine-reactive fluorescent dye non-permeant cells (H).

**I, J.** sgCBX4-mediated CBX4 knockout efficiencies in J-Lat 10.6 cells were evaluated by western blot (I). Cellular viabilities upon CBX4 knockout were evaluated by measuring the percentages of amine-reactive fluorescent dye non-permeant cells (J).

Data information: Data represented mean ± SEM in biological triplicate. p-Values in (A), (C), (F), (H) and (J) were calculated by Student's *t*-test. p-Values in (E) were calculated by two-way ANOVA with Tukey's multiple comparisons test. $^{**}p < 0.01$, $^{***}p < 0.001$.

# Appendix Figure S3. CBX4 forms nuclear condensates.

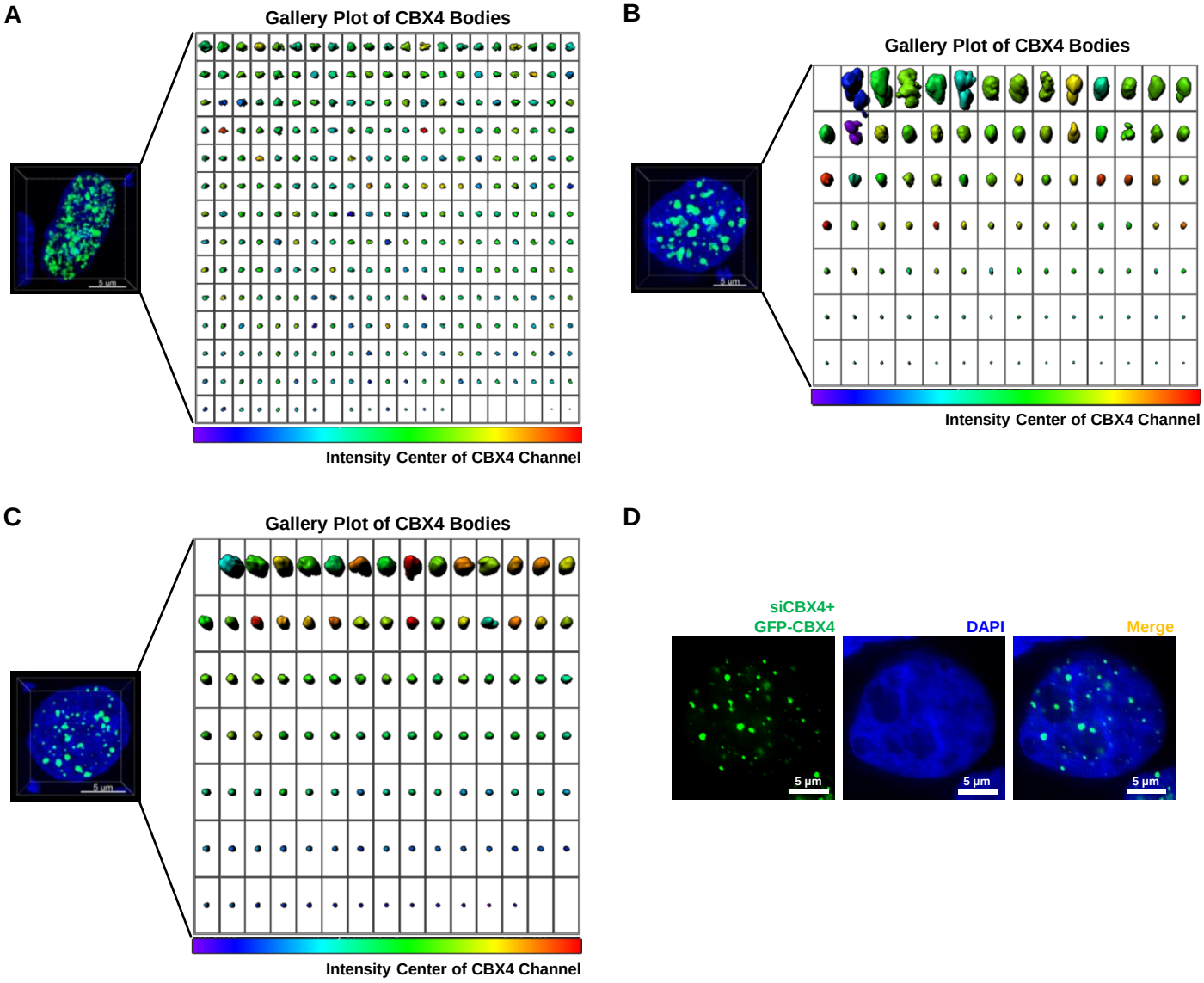


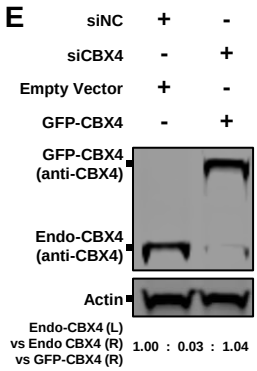


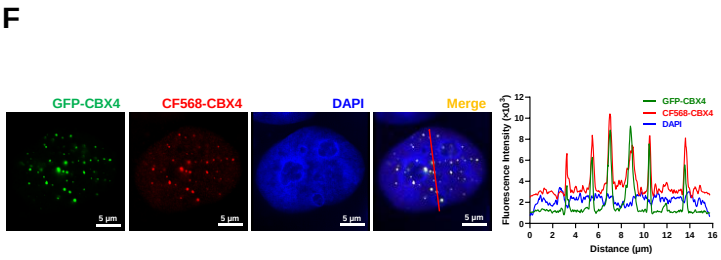


**Appendix Figure S3. CBX4 forms nuclear condensates.**

**A-C.** The 3D-Stack images of CBX4 bodies within three representative HEK293T cells. All the bodies were analyzed by Imaris software and aligned according to their sizes, which were shown as gallery plots on the right of each panel. The colors of CBX4 bodies indicated the intensity center of CBX4 channel.

**D.** The endogenous CBX4 in HEK293T cells was knocked down by siRNAs targeting 3' UTR of *CBX4* mRNA. About 24 hours post siRNAs-transfection, cells were transfected with GFP-CBX4. The expression and distribution of GFP-CBX4 were evaluated by SIM imaging. DAPI was used to dye DNA which was colored into blue.

**E.** The efficiencies of CBX4 knockdown and GFP-CBX4 expression in (D) were evaluated by western blot. The expression ratio of endogenous CBX4 and GFP-CBX4 within both groups was calculated. "L" represented left group. "R" represented right group.

**F.** HEK293T cells were transfected with GFP-CBX4-expressing plasmids. The expression of CBX4 was evaluated by both GFP expression and CBX4 primary antibodies. CF568-conjugated secondary antibodies were used to detect primary antibodies-captured CBX4. The line scan profile was shown on the right. The red arrow indicated the profiled position.

**G.** The expression of endogenous CBX4 and GFP-CBX4 was evaluated by western blot with antibodies against CBX4. The expression ratio of endogenous CBX4 and GFP-CBX4 within both groups was calculated and marked below the figure. "L" represented left group. "R" represented right group.

Data information: Scale bars in (A-D) and (F) represented 5 μm.

# Appendix Figure S4. CBox of CBX4 mediated the LLPS of CBX4 bodies.

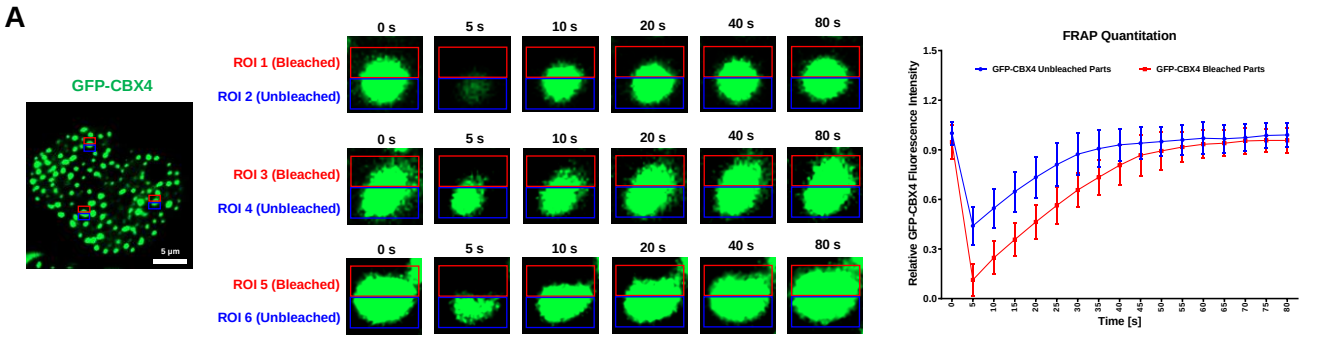


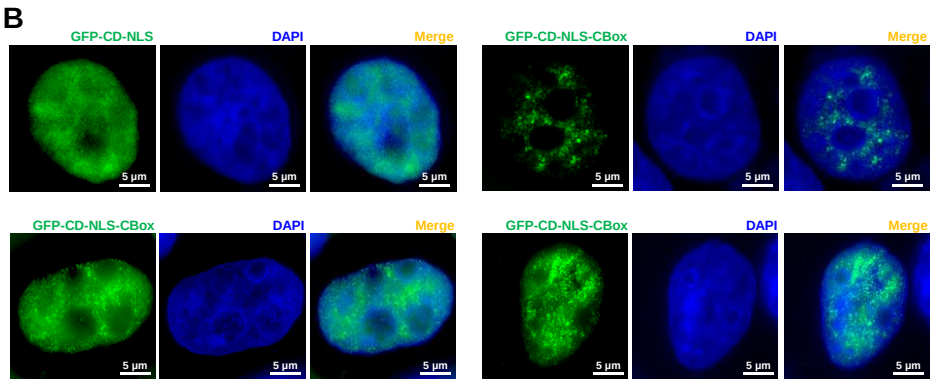


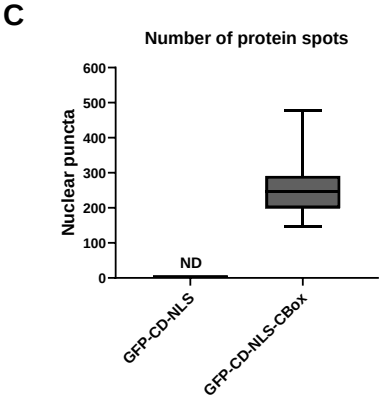


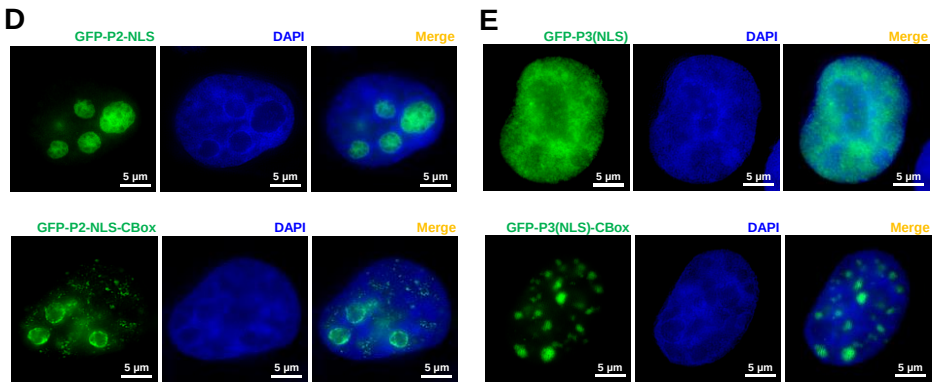





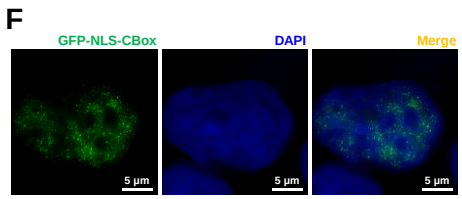

**Appendix Figure S4. CBox of CBX4 mediated the LLPS of CBX4 bodies.**

**A.** FRAP images of CBX4 bodies. Three GFP-CBX4 bodies were split into two parts. Only half parts of these bodies were bleached and marked as ROI 1, ROI 3 and ROI 5. Another half parts were unbleached and marked as ROI 2, ROI 4 and ROI 6. Images were captured every 5 s. The right histogram showed relative fluorescence intensities of both unbleached and bleached parts in each time point.

**B, C.** Different GFP-tagged CBX4 mutants including CD-NLS and CD-NLS-CBox were overexpressed in HEK293T cells and imaged with SIM. Data showed one cell which expressed GFP-CD-NLS and three cells which expressed GFP-CD-NLS-CBox (B). The numbers of nuclear puncta within both groups were calculated with Imaris (C).

**D-F.** Different GFP-tagged CBX4 mutants including P2-NLS, P2-NLS-CBox, P3(NLS), P3(NLS)-CBox and NLS-CBox were overexpressed in HEK293T cells and imaged with SIM.

Data information: Scale bars in (A), (B) and (D-F) represented 5 μm. All the samples were imaged to obtain at least three sets of images. Data represented mean ± SEM in biological triplicate in (A). Data in (C) represented puncta numbers in biological replicate (n=8). The central band of the boxplot represented median values of puncta numbers. The height of the box represented the interquartile range of puncta numbers. The boundaries of the upper whisker and the lower whisker represented the maximum number and the minimum number, respectively.

**Appendix Figure S5. Knockdown efficiencies and cellular viabilities in SUMOylation assay.**

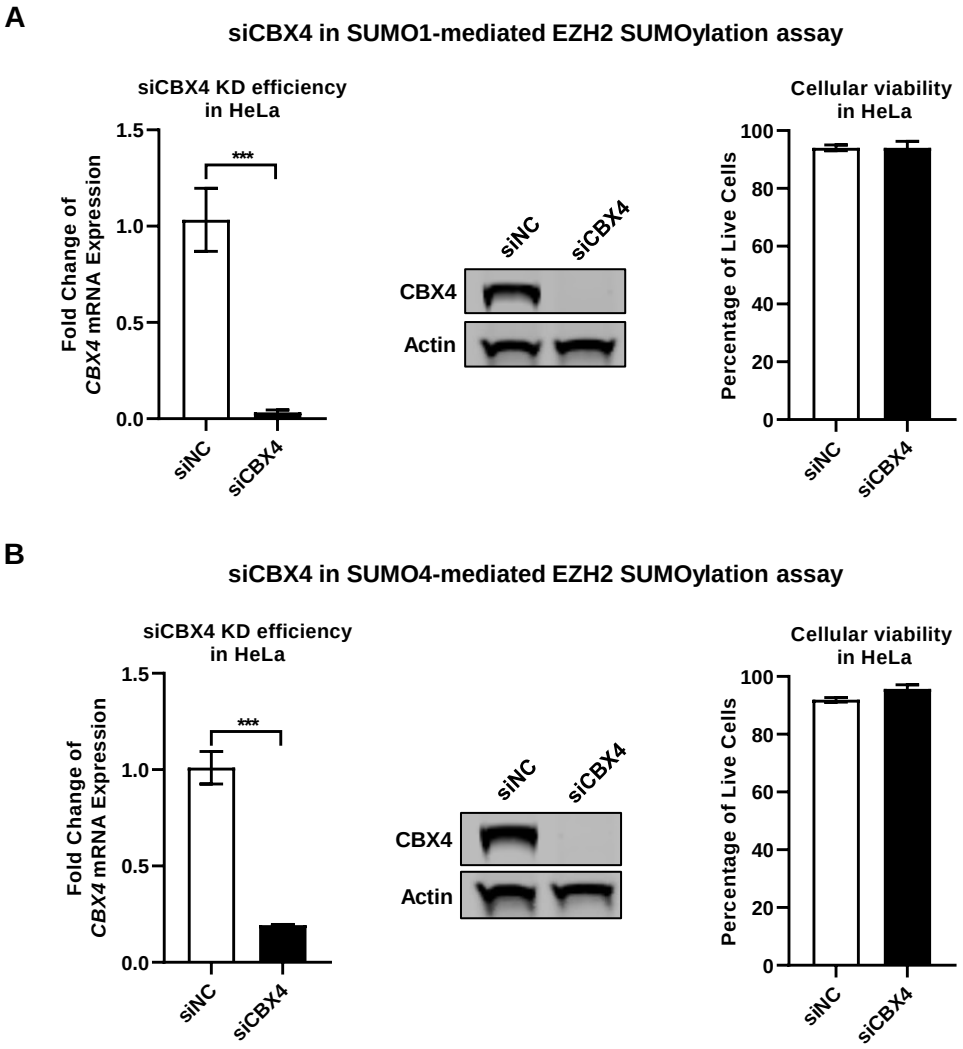

**Appendix Figure S5. Knockdown efficiencies and cellular viabilities in SUMOylation assay.**

**A.** siCBX4-mediated CBX4 knockdown efficiencies in SUMO1-mediated EZH2 SUMOylation assay were evaluated by both RT-qPCR (left subpanel) and western blot (middle subpanel). Cellular viabilities upon CBX4 knockdown in HeLa cells were quantitated by measuring the percentages of amine-reactive fluorescent dye non-permeant cells (right subpanel).

**B.** siCBX4-mediated CBX4 knockdown efficiencies in SUMO4-mediated EZH2 SUMOylation assay were evaluated by both RT-qPCR (left subpanel) and western blot (middle subpanel). Cellular viabilities upon CBX4 knockdown in HeLa cells were quantitated by measuring the percentages of amine-reactive fluorescent dye non-permeant cells (right subpanel).

Data information: Data represented mean ± SEM in biological triplicate. p-Values were calculated by Student's *t*-test. ***$p < 0.001$.

# Appendix Figure S6. The influence of CBX4 and mutants on HIV-1 suppression.

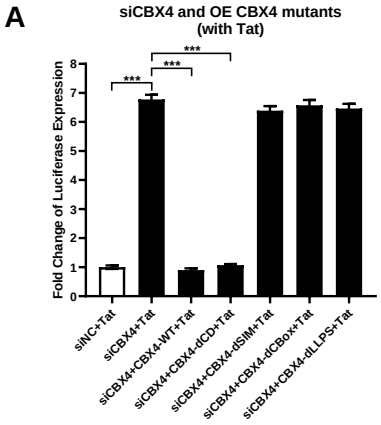


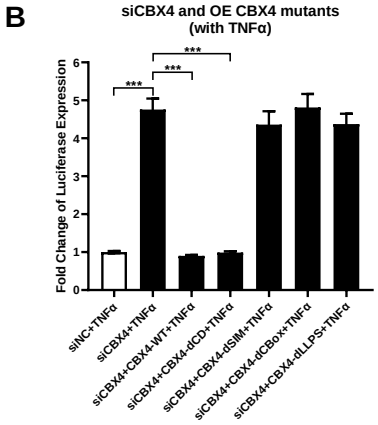


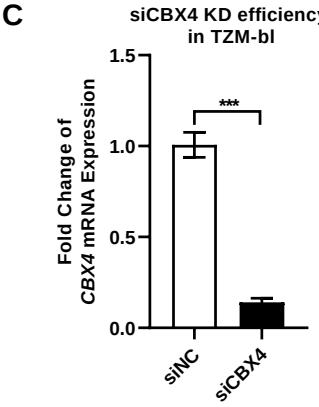


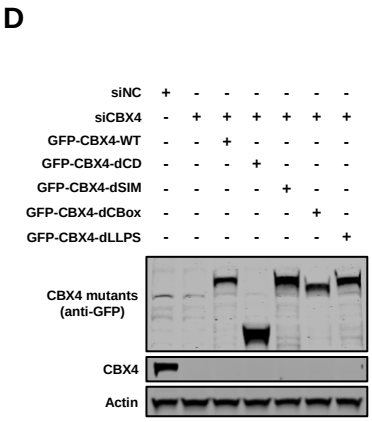


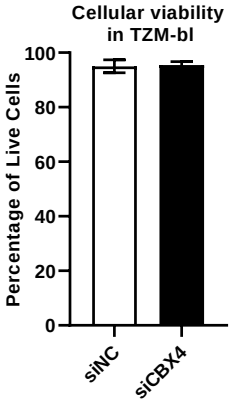


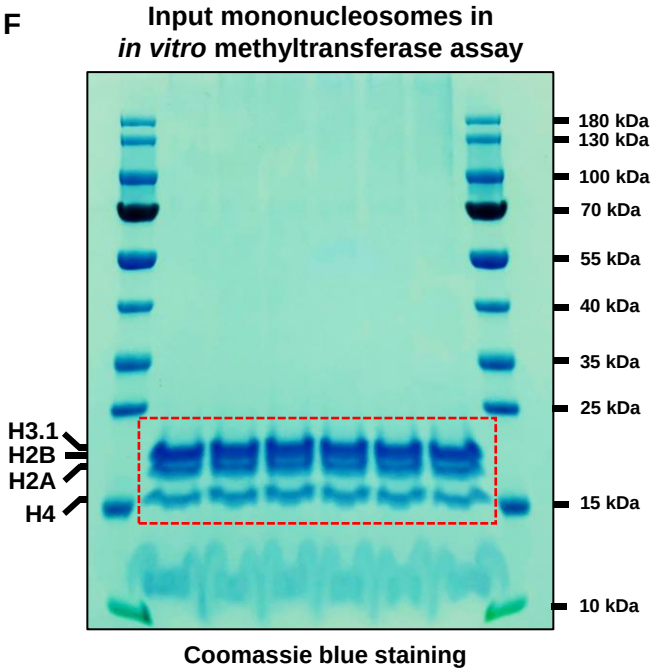

**Appendix Figure S6. The influence of CBX4 and mutants on HIV-1 suppression.**

**A.** TZM-bl cells were treated with siCBX4 targeting the 3'UTR of *CBX4* mRNA. About 24 hours later, cells in each group were transfected with different CBX4 mutants and equal amounts of Tat-expressing plasmids. Another 24 hours later, cells were proceeded to luciferase assay.

**B.** TZM-bl cells were treated with siCBX4 and overexpressed with different CBX4 mutants. About 24 hours post transfection, cells in each group were treated with TNFα. Another 24 hours later, cells were proceeded to luciferase assay.

**C-E.** The knockdown efficiencies of siCBX4 in TZM-bl cells were confirmed by both RT-qPCR (C) and western blot (D). The overexpression of CBX4 and corresponding mutants was confirmed by western blot (D). Cellular viabilities upon CBX4 knockdown by siCBX4 in TZM-bl cells were evaluated by measuring the percentages of amine-reactive fluorescent dye non-permeant cells (E).

**F.** The purities of input mononucleosomes in the *in vitro* methyltransferase assay, which was conducted in Fig 6E, were evaluated by Coomassie blue staining. Red dashed line-circled region which indicated H3.1, H2B, H2A and H4 was also showed in Fig 6E.

Data information: Data represented mean ± SEM in biological triplicate. p-Values in (A) and (B) were calculated by one-way ANOVA with Tukey's multiple comparisons test. p-Values in (C) and (E) were calculated by Student's *t*-test. ***$p < 0.001$.

# Appendix Figure S7. CBX4 knockdown efficiency and cellular viability in CD4$^+$ T cells.

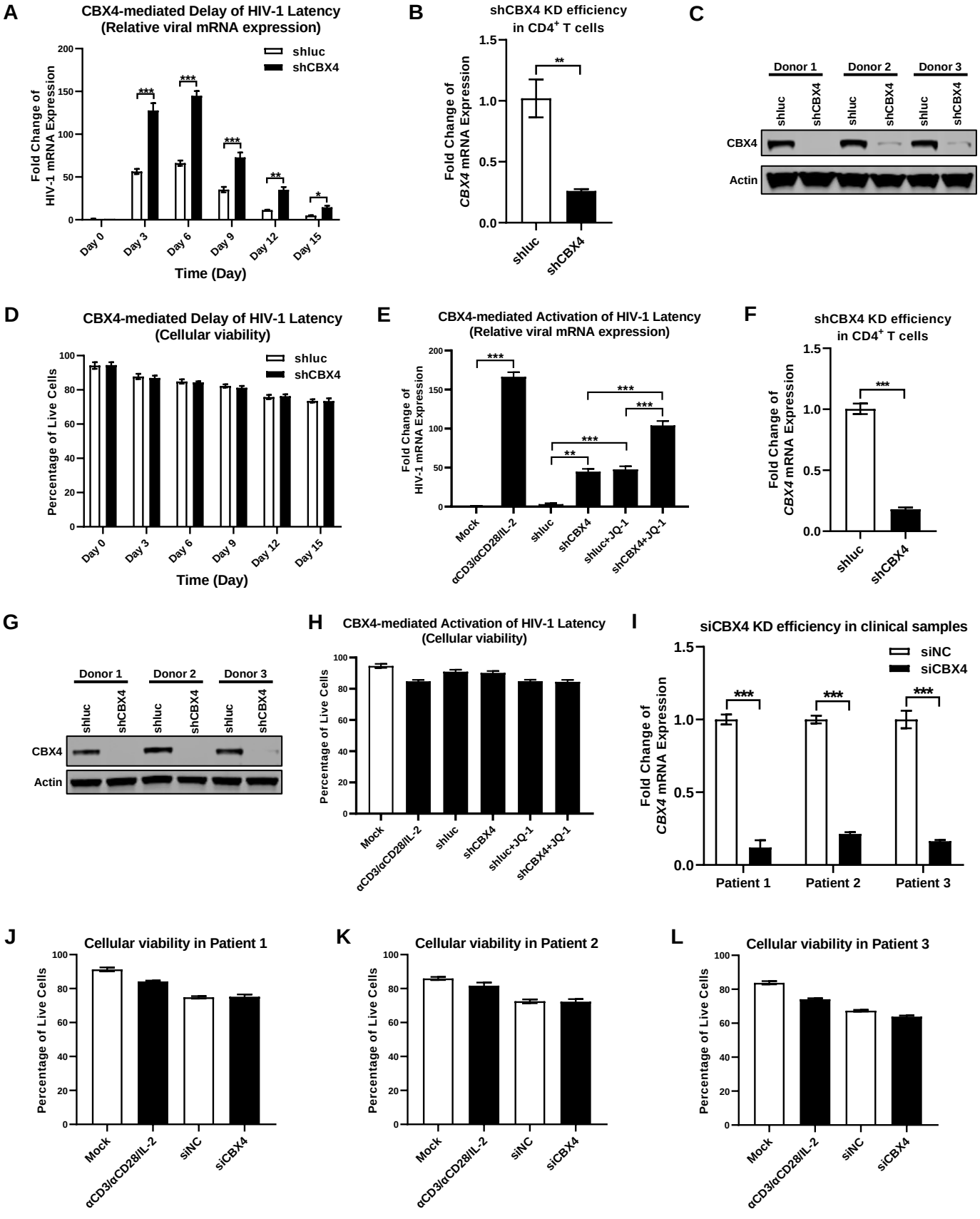

**Appendix Figure S7. CBX4 knockdown efficiency and cellular viability in $CD4^+$ T cells.**

**A.** Primary $CD4^+$ T cells were treated as in Fig 7A. The expression of HIV-1 mRNA within each group was quantitated and normalized to that on Day 0.

**B-D.** The efficiencies of shCBX4-mediated CBX4 knockdown in $CD4^+$ T cells on Day 6 were evaluated by both RT-qPCR (B) and western blot (C). Cellular viabilities within each time point in both shluc and shCBX4 groups were evaluated by measuring the percentages of amine-reactive fluorescent dye non-permeant cells (D).

**E.** Primary $CD4^+$ T cells were treated with shluc and shCBX4 as in Fig 7D. The relative HIV-1 mRNA expression in each group was quantitated by RT-qPCR and normalized to that in Mock group.

**F-H.** The efficiencies of shCBX4-mediated CBX4 knockdown in Fig 7D were evaluated by RT-qPCR (F) and western blot (G). Cellular viabilities in each group were evaluated by measuring the percentages of amine-reactive fluorescent dye non-permeant cells (H).

**I.** The efficiencies of siCBX4-mediated CBX4 knockdown in three clinical samples which were used in Fig 7E-G were evaluated by RT-qPCR.

**J-L.** Cellular viabilities within each group of three clinical samples were evaluated by measuring the percentages of amine-reactive fluorescent dye non-permeant cells.

Data information: Data represented mean ± SEM in biological triplicate. p-Values in (A), (D) and (I) were calculated by two-way ANOVA with Sidak's multiple comparisons test. p-Values in (B) and (F) were calculated by Student's *t*-test. p-Values in (E), (H) and (J-L) were calculated by one-way ANOVA with Tukey's multiple comparisons test. *$p < 0.05$, **$p < 0.01$, ***$p < 0.001$.